Sports Engineering (2020) 23:5
https://doi.org/10.1007/s12283-020-0319-0

ORIGINAL ARTICLE

When can you expect contrast swing in a cricket game, and how to obtain it?

Loïc Tadrist[1] · Naresh Sampara[1] · Intesaaf Ashraf[2] · Thomas Andrianne[1]

Published online: 25 February 2020

Abstract
Curved trajectories are widely used in sports played with balls. Specifically, in cricket, balls are bowled with curved trajectories to surprise the batsman. Amongst the bowling techniques that provide curved trajectories, one of the most controversial is called *contrast* swing. This technique is specific to cricket and happens when the ball gets a nonuniform wear on each hemisphere after a few launches. The differential wear on the two sides of the cricket ball creates an aerodynamic side force. We quantify this force through wind tunnel experiments varying the roughness on one hemisphere of the ball. Trajectory modelling shows that this aerodynamic force is consistent with measurements on real throws. We also measure the side-to-side differential wear generated on a cricket ball as a function of the number of launches. Finally, we estimate the minimum velocity required to achieve *contrast* swing and the expected deviation as a function of launches number and game conditions.

Keywords Contrast swing · Cricket aerodynamics · Roughness

1 Introduction

For most ball sports, aerodynamics is the key physical feature to predict ball trajectory [1, 2]. Amongst ball sports, football is a good example where curved ball trajectories are advantageously used to trick the opponent [3, 4]. Similarly to football, tennis players use curved trajectories by spinning the ball, using the Magnus effect [5]. In cricket, the Magnus effect is also used by spin bowlers [6]. However, the nature of a cricket ball surface is peculiar. It consists of two hemispheres covered by a smooth piece of waxed leather sewn to the ball close to the equator. For this reason, additional physical effects may be used to bend the ball trajectory.

Most of the time, bowlers launch the ball with the seam inclined with respect to the ball trajectory. Since the seam sticks out few hundreds of microns above the leather, it modifies the boundary layer flow on one side of the cricket ball. This creates a lateral aerodynamic force that bends the ball trajectory [7, 8]. This effect is called *classic* swing [6, 9]; see Fig. 1a. Players have adapted to this launching technique and anticipate the in-swinging or out-swinging trajectory of the ball according to the initial seam position.

Another technique used by the bowlers is *contrast* swing as named by Mehta [6, 10]. Contrast swing is the simplest configuration where roughness effects appear since the trajectory is initially included in the seam plan; Fig. 1. Contrary to classic swing, the seam does not play a major role in contrast swing. Reverse swing is somehow similar to contrast swing,but in a more complex configuration where the trajectory is not included in the seam plane; Fig. 1c. There have been many legends concerning the contrast and reverse swing techniques, but it is now well accepted that it may only appear when the ball is worn differently on each hemisphere [6, 11], see Fig. 1. Roughness is indeed a key parameters for sport ball aerodynamics [12–14]. Things get interesting both on a scientific and a sportive point of view when differential roughness appears on the ball.

✉ Loïc Tadrist
loic.tadrist@uliege.be

Naresh Sampara
naresh.sampara@gmail.com

Intesaaf Ashraf
i.ashraf@uliege.be

Thomas Andrianne
t.andrianne@uliege.be

[1] Department of Aerospace and Mechanics, University of Liège, Allée de la découverte 9, 4000 Liège, Belgium

[2] GRASP, Physics Department B5a, University of Liège, 4000 Liège, Belgium

Although confusing for the batsman, contrast swing is not often used in the field since it requires a ball worn on only one hemisphere. Contrast swing usually bends the ball trajectory towards the rough side, but when launched at high speed, $U > 31\,\mathrm{m\,s^{-1}}$, the swing direction may be reversed [10].

Contrast swing relies on an asymmetric flow around the ball due to the differential roughness. Depending on roughness, the boundary layer may transit from laminar to turbulent at different critical Reynolds numbers. The critical Reynolds number R_e^* has been studied by Achenbach [15] to quantify drag crisis on a rough sphere. The critical Reynolds number R_e^* decreases as the roughness r of the ball increases. Contrast swing takes place when the rough side of the ball has a turbulent boundary layer and the boundary layer of the smooth side of the ball is still in the laminar regime. At a given Reynolds number, the turbulent boundary layer (rough side) remains attached to the ball further than the laminar boundary layer (smooth side). This break of symmetry creates a side force that bends the ball trajectory towards the rough side.

At high bowling velocity, $U > 31\,\mathrm{m\,s^{-1}}$, both the rough side and the smooth side are turbulent. Now, it is the smooth side boundary layer that detaches further than the one of the rough side. The direction of the contrast swing is thus reversed towards the smooth side. In the following, we only focus on the low-speed contrast swing, for which the physics can also be used to discuss the high speed contrast swing.

Although cricket ball aerodynamics has been largely discussed [6, 7, 11, 16, 17], game conditions to produce contrast or reverse swing, Fig. 1b and c, have never been analysed quantitatively except in Scobie et al. [14, 18]. We propose here to examine the contrast swing technique's dependence on ball roughness by using both experimental and theoretical approaches. We predict the necessary game conditions to produce contrast swing in terms of the number of launches and launching velocity.

First, we performed wind tunnel experiments to measure the aerodynamic drag and side forces due to the differential roughness. This original data directly relates the side force appearance to the drag crisis and is complementary of the measurements of Sayers [16] and Scobie et al. [14]. Then we quantified the effect of differential roughness on the lateral aerodynamic force, both in magnitude and critical velocity (i.e. the velocity corresponding to the drag crisis). We also measured the wear of a cricket ball as a function of the number of launches to be able to link it to ball roughness. Finally, we implemented those measurements in a model of the ball trajectory, similarly to Baker [19]. We predict the minimal launching velocity to achieve contrast swing and the expected lateral deviation as a function of roughness. We also predict at which point of the cricket game (*i.e.* number of launches after a new ball was introduced) contrast swing can happen.

2 Materials and methods

We performed wind tunnel measurements of the side force created by the roughness difference between the two hemispheres of the ball. Four cricket balls (Boom prime, grade A supreme test professional red leather) and one field hockey ball (Dita®, Hockey ball) were tested in the wind tunnel. One cricket ball was kept untouched and the three other were machined to create a uniform roughness on one hemisphere. The cricket balls were 7.0 cm in diameter. The field hockey ball was chosen because its dimensions were similar to the cricket ball (7.1 cm in diameter) and its surface was smooth (obtained by plastic moulding). It was used as a reference smooth ball/sphere.

Another cricket ball was used to determine the wearing rate of a cricket ball by repeatedly launching it on a pitch, as would happen in a cricket game.

2.1 Trajectory measurements

The trajectory measurements, Fig. 2, were performed indoor to prevent any external draft that may deviate the ball. A camera (*GoPro*™ Hero 3+) was fixed 6 m above the pitch and recorded launches with a resolution of 1080p at 60 frames per second.

The balls were launched by a non-professional bowler. The bowler was recruited amongst faculty members, informed with the details of the study and signed consent before participation. The study conformed to the ethical procedures of the University of Liège. Special care was taken to have the ball spin vector perpendicular to the seam plane and the trajectory direction included in the seam plane, $\theta = 0 \pm 5°$, Fig. 1b. Two cricket balls have been tested, one unworn ball and a second one with one hemisphere uniformly worn using a drill machine (Dremel®4000). The unworn ball had a surface made of smooth waxed leather with a peak-to-peak roughness of 6 µm. The ball was launched ten times and became increasingly worn after each launch of the trial. The machined ball had a peak-to-peak roughness of ≈ 1 mm and was also launched three times without much alteration of its rough hemisphere.

The trajectories were processed automatically (Matlab code) to extract the lateral deviation δ on the field of view of the camera (around 6 m) and the initial velocity of the ball, U_0. Image calibration was done using four reference points. The launching speed U_0 and the lateral deviations δ were in the range 18–22 m s^{-1} and 0–0.20 m, respectively. The resolution was 4 mm per pixel, but the ball appeared blurry on the images because of its speed. This resulted in a

large uncertainty on the ball position, ± 5 cm in both x and y directions. The trajectory of the unworn ball was not perfectly straight because it was launched by a non-professional bowler with some uncertainty on the seam direction, and because it became increasingly worn with each trial. Even with those uncertainties, the trajectories between those two balls were different.

2.2 Roughness measurement

Different definitions of roughness exist in the literature; see [12]. Here, we choose Achenbach's definition [15],

$$r = \frac{k}{d}, \tag{1}$$

where k is the peak-to-peak value of the surface elevation and d is the ball diameter. k is measured as the difference between the deepest hollow and the largest protrusion regarding the position of the mean surface. Roughness measurements were carried out with a conventional roughness meter (Hexagon metrology, Rugosurf 20). For each ball, the peak-to-peak roughness was measured at five random locations on patches of 6.5 mm^2. The smallest and largest values were then discarded to exclude rare events from the definition of ball roughness. The wind tunnel tests were performed on five balls: four cricket balls, unworn $r = 0.85 \pm 0.4\,10^{-4}$, small roughness $r = 4.75 \pm 2.1\,10^{-4}$, middle roughness $r = 1.0 \pm 0.4\,10^{-3}$ and large roughness surfaces $r = 1.4 \pm 1.0\,10^{-2}$, and a smooth field hockey ball of roughness $r = 2.55 \pm 2.5\,10^{-5}$, see Fig. 3. The cricket balls were machined as follows to create uniform roughness on one hemisphere. Some patches of wax were removed on the ball with small roughness. Those patches represented approximatively 30% of the surface of the ball hemisphere and were uniformly distributed. For the middle roughness ball, all the wax was removed with sand paper grain 60. Finally, the large roughness ball was drilled (Dremel®4000 fitted with a diamond grinding wheel) on approximatively 50% of its surface with hollow patches of 1 mm deep, 7 mm long and 3 mm wide. These methods used to create controlled roughness might not be representative of the wear of a cricket ball during play.

The measurements of the ball roughness evolution as a function of the number of launches was performed every three launches. The launches were performed on a dry ground with similar consistency to a cricket pitch (compacted ground on which the cricket ball was rising up to the shoulder of the wicketkeeper). The similar roughness measurement procedure was then applied as for the balls studied in the wind tunnel. This method wears the ball in a similar manner to that in a cricket match, but the wear rate may vary from one pitch to another and with weather conditions.

2.3 Wind tunnel tests

The balls were tested in the aeronautical test section (2 m × 1.5 m) of the wind tunnel laboratory of the University of Liège; see [20] for details. The wind velocity was measured with a Pitot tube with an accuracy of ± 0.1 m s^{-1}. The aerodynamic forces applied to the ball were measured by a six component load sensor (nano17 by ATI^{TM}) at 500 Hz with an absolute accuracy of ± 0.0125 N. The sensor was screwed to the ball on the seam in the leeward face to minimize its effect on the measurement. Special attention was paid to align the seam with the airflow ($\theta = 0$), in a contrast swing fashion, to avoid the effect of the seam. The ball was supported by a sting of diameter 18 mm and a vertical pole situated 80 cm downstream; see Fig. 3. Turbulence intensity in the wind tunnel was 0.2% and blockage ratio was 0.13%.

3 Aerodynamic forces on a cricket ball

For each ball, the drag C_D, the lift C_L and the side C_S coefficients were measured and plotted as a function of the wind velocity in Fig. 4. For the smooth hockey ball that we used as a reference ball, the drag coefficient C_D remained similar to the Achenbach [15] measurements for a smooth sphere at all wind speeds; see Fig. 4a. No drag crisis was observed. For the cricket balls with differential roughness but also for the unworn cricket ball, the drag crisis occurred. It took place at different wind speeds depending on roughness.

The side coefficient C_S was influenced by the differential roughness of the ball. The field hockey ball had no protuberances on its surface and no significant side forces were measured at any wind speed as expected. The cricket balls with differential roughness, however, suffered a transition from no side force at low wind velocities to side force as the wind speed was increased; see Fig. 4b. The side force was taken positive from the smooth hemisphere to the rough one. The transition from no side force to side force occurred at different wind velocities which decreased as the roughness was increased. Finally at high wind velocity, the balls met a new transition with a reversal of side force. For the unworn ball, C_S remained close to 0 for low wind speeds, but followed a similar transition as the worn cricket balls with an increase of C_S up to 0.4 before it returned to 0 for wind velocities larger than 50 m s^{-1}. This behaviour breaks the apparent symmetry of the ball; nevertheless, it was reproducible for different new cricket balls. Since we were not able to observe such a behaviour on the smooth hockey ball which was also symmetrical, we interpret this change as the non-perfect symmetry of a new cricket ball. The cricket ball used in the experiment was hand-made, and the seam protuberance and also the brand prints on the side may trigger this change. The side force on the unworn cricket ball appears at

velocities higher than 40 m s^{-1}, which are only met by fast professional bowlers [21].

As expected, the value of the lift coefficient C_L is close to 0 for all the balls as a consequence of their symmetry along the horizontal plane (perpendicular to the seam of the ball); see Fig. 4c.

We isolate the aerodynamic force coefficients applied on the cricket ball with small differential roughness; see Fig. 5. The drag coefficient drops down for the first time at a velocity of 29 m s^{-1}. At this point, the side coefficient jumps to 0.4. between 29 and 45 m s^{-1}, C_D and C_S are constant. After 45 m s^{-1} the drag coefficient decreases again to 0.3 and the side force is inverted $C_S = -0.25$. We interpret the first jump as the transition of the boundary layer from laminar to turbulent on the rough side of the cricket ball and the second jump to the transition on the smooth side of the cricket ball. Thus, the white region in Fig. 5 corresponds to a laminar boundary layer on both sides of the ball. The light grey region corresponds to a turbulent boundary layer on the rough side of the ball and a laminar boundary layer on the smooth side of the ball. Finally, the grey region corresponds to both boundary layers being turbulent. The experimental data and the above explanation support the view of Mehta [10] about contrast swing.

From Fig. 4, it is possible to extract the effect of roughness on the aerodynamic performance of the balls. The ratio of the side coefficient to the drag coefficient is plotted in Fig. 6. In the case of balls with differential roughness (blue, orange and red stars), the maximum value of this ratio, $|C_S/C_D| \in [0.5;1]$, is reached at different wind speeds. Except for velocities larger than 40 m s^{-1}, the ratio is five times smaller in the case of the unworn ball ($|C_S/C_D| < 0.2$), while the hockey ball has an almost null ratio $|C_S/C_D| \simeq 0$. The differential roughness mainly increases the side force which bends the trajectory.

3.1 Wear of the cricket ball

The cricket balls tested in the wind tunnel were machined to obtain a uniform and high roughness on one hemisphere. However, in game conditions, the cricket balls are worn by successive impacts on the ground. The roughness appears by patches of approximatively 4 cm^2. Depending on the number of launches, those patches populate the cricket ball surface. When the impact occurs several times at the same location, it deepens the wrinkles on the ball and thus increases local roughness. Thus, mean ball roughness increases by both surface wear and roughness depth. We conducted wear tests of a cricket ball after it had impacted several times on a compacted ground similar to a cricket pitch. The ball was launched on the ground with an impact at approximatively 10 m in front of the non-professional launcher. The ball velocity was not controlled, but almost fixed to the maximal speed achievable by the bowler ($\simeq 30\,\mathrm{m\,s^{-1}}$). The bowler repeatedly oriented the ball to impact on the same hemisphere. The results are displayed in the inset of Fig. 7. The wear values increased with the number of launches.

4 Model

To compute the trajectory of the ball and the expected deviation as a function of ball roughness, we built a model based on the aerodynamic forces measured in the wind tunnel. We assumed the ball to be in a contrast swing configuration, Fig. 1b, to simplify our modelling. The ball was launched with the seam vertically aligned with the trajectory direction ($\theta = 0$). We also assumed that the ball was spinning along the seam. In this configuration, the Magnus effect only acted on the vertical motion of the ball, and no horizontal displacement was expected. The Magnus effect was thus not taken into account in our 2D model, in which we also neglected gravity. In this section, we first computed the variation of the yaw angle θ and showed that it remained small. Subsequently, we developed a ballistic model to predict lateral deviation as a function of launching velocity and ball roughness.

4.1 Gyroscopic effect

We model here the horizontal trajectory of a cricket ball, assuming that the ball is spinning in the seam plane. The angular velocity vector $\boldsymbol{\omega}$ is orthogonal to the ball trajectory and horizontal; Fig. 1b.

The drag on the smooth side $\rho C_D U^2 \pi d^2/16$ is larger than the drag on the rough side $\rho C_D^* U^2 \pi d^2/16$, since from Fig. 4 we can estimate $C_D \simeq 0.5$ and $C_D^* \simeq 0.4$. The lever arm may be computed as

$$\frac{2}{\pi d^2} \int_0^{d/2} 2\pi \sqrt{\frac{d^2}{4} - z^2} \quad z \, \mathrm{d}z = \frac{d}{6}. \tag{2}$$

This configuration creates an aerodynamic torque τ that spins the ball around the vertical axis z, Fig. 1. It reads

$$\tau = \pi \frac{C_D - C_D^*}{96} \rho \, U_0^2 d^3. \tag{3}$$

The spinning of the sphere around the z axis follows the conservation of angular momentum $\vec{\tau} = \mathrm{d}\vec{L}/\mathrm{d}t$. The angular momentum of the ball is given by $\vec{L} = I\vec{\omega}$, where I is the rotational inertia of the ball and $\vec{\omega}$ the spinning vector. Assuming that the cricket ball is a sphere with uniform density, $I = m\,d^2/10$. The effect of this aerodynamic torque does not change the magnitude of $\vec{L}$ but only its direction, since $\vec{L}$ and $\vec{\tau}$ are orthogonal. The change in yaw angle θ over

a distance D (pitch length), for a ball launched with initial velocity U_0, is obtained from

$$\theta \approx \frac{\tau D}{U_0 I \omega} = \frac{5\pi (C_D - C_D^*)\rho U_0 d D}{48 m \omega}. \quad (4)$$

The spin rate of cricket bowlers ranges between 2 and 37 rotations per second after ball release [16, 22–24], with a typical value of 25 rps. Taking $\omega = 50\pi$ rad s^{-1}, $C_D = 0.5$, $C_D^* = 0.4$ and initial velocity $U_0 = 20$ m s^{-1}, one computes $\theta = 2.5°$. The gyroscopic effect provided by the spinning of the ball reduces the change in yaw angle θ. This small change of yaw angle, of a few degrees, may affect the aerodynamics forces applied on the ball. Nevertheless, those effects are small compared to the effect of roughness [11, 16]. In the following, we neglect the variation of orientation of the ball, considering that the seam always remains parallel to the launch direction.

4.2 Lateral deviation of the ball

For simplicity, we consider that the ball velocity is mainly in the x-direction, $\dot{x} \gg \dot{y}$. In the horizontal plane, the ball is only subjected to aerodynamic forces, namely the drag force and the side force. Conservation of momentum in the x-direction and y-direction yields:

$$m\ddot{x} = -\pi\rho C_D \dot{x}^2 d^2/8 \quad \text{and} \quad m\ddot{y} = -\pi\rho C_S \dot{x}^2 d^2/8. \quad (5)$$

We suppose here, as a first step, that the launching velocity is above the critical velocity $U_0 > U_c$ and that both C_S and C_D are constant and do not depend on the ball velocity. The drag coefficient C_D slightly decreases with the ball spinning velocity by about 10% ([25, 26]), but it can still be treated as a constant since the decrease of spinning velocity is negligible during the flight. This set of equations is solved to obtain the ball trajectory $x(t)$ and $y(t)$:

$$\frac{x}{U_0 t_d} = \ln\left(1 + \frac{t}{t_d}\right) \quad (6)$$

and

$$\frac{y}{U_0 t_d} = \frac{C_S}{C_D}\left(\ln\left(1 + \frac{t}{t_d}\right) - \frac{t}{t_d}\right), \quad (7)$$

where $t_d = 8m/\pi\rho C_D d^2 U_0$ is defined as the typical deceleration time. Note that the value of t_d is 7.64 s for a launching velocity $U_0 = 20$ m s^{-1} and for the parameters value given in Table 1. This value is much larger than the actual flying time of the ball over the cricket pitch, which is around 1 s. This means that the ball velocity does not decrease much during the flight $\dot{x} \approx U_0$. With the approximation $t \ll t_d$, we obtain the lateral displacement at pitch length D,

$$\delta = -\frac{C_S}{2C_D}\frac{D^2}{U_0 t_d} = -\frac{\pi\rho C_S d^2 D^2}{16m}. \quad (8)$$

With the assumption of constant C_S and C_D, the lateral displacement does not depend on launching velocity. We can refine this model by specifying that C_S depends on U_0, as plotted in Fig. 4b. We curve fit the experimental data in that figure using the following model:

$$C_S = \frac{C_S^*}{2}\big(1 + \tanh[\alpha(U_0 - U_c - \beta)]\big), \quad (9)$$

where C_S^* corresponds to the asymptotic value of C_S for high U_0 and α is the transition slope and $U_c - \beta$ the centre of the transition zone (U_c corresponds to the beginning of the transition). Fitting this model to the high roughness data of Fig. 4,b we obtain $C_S^* = 0.33$, $\alpha = 0.33$ s m^{-1} and $\beta = 3.5$ m s^{-1}.

Mehta [6, 11] showed that the appearance of a side force is linked to the change of flow regime in the boundary layer of the rough side of the ball. The boundary layer transitions from laminar to turbulent [7, 14] and the position of the separation point moves downstream. The boundary layer on the smooth side of the ball remains laminar, resulting in a flow asymmetry between the two hemispheres and causing a significant side force. The transition from laminar to turbulent boundary layer is also known to trigger the drag crisis on a bluff body [15]. Achenbach showed that the critical Reynolds number at which the drag crisis occurs decreases for rougher spheres. We define the critical Reynolds number R_e^* when the drag coefficient C_D is smaller than 0.4, which corresponds to the beginning of the drag crisis. We plot the critical Reynolds number R_e^* as a function of roughness r in Fig. 8. We define the Reynolds number and the critical Reynold number as

$$R_\mathrm{e} = \frac{Ud}{\nu} \quad \text{and} \quad R_\mathrm{e}^* = \frac{U_c d}{\nu}, \quad (10)$$

where U is the wind velocity, U_c the critical velocity, d the ball diameter and ν the air kinematic viscosity. The critical velocity U_c is defined as the wind velocity at the centre of the transition zone, and it depends on the roughness of the ball. Achenbach's data ([15]) and our wind tunnel results are compared in Fig. 8. All data gather on a line on a log-lin diagram. The critical Reynolds number R_e^* of transition from laminar to turbulent boundary layer decreases with the roughness r. We fit the critical Reynolds number R_e^* with an empirical law,

$$R_\mathrm{e}^* = A\log(r) + B, \quad (11)$$

Table 1 List of parameters and values for cricket balls used in this paper

	Cricket parameters	Typical value
m	mass of the cricket ball	0.156 kg
d	Cricket ball diameter	$7.0\,10^{-2}$ m
D	Pitch length	18.9 m
I	Rotational inertia	$7.6\,10^{-5}$ kg.m^2
U_0	Launching velocity	15–45 m s^{-1}
$\vec{\omega}$	Spin vector	$50\,\pi$ rad s^{-1}
k	Peak-to-peak defect size	µm – mm
r	Roughness	$10^{-5} - 10^{-2}$
	Aerodynamics parameters	Typical value
ρ	Air density	1.23 kg m^{-3}
ν	Air kinematic viscosity (20 °C)	$1.5\,10^{-5}$ m^2 s^{-1}
C_D	Drag coefficient	0.4
C_L	Lift coefficient	0
C_S	Side coefficient	–
R_e	Reynolds number	10^5
R_e^*	Reynolds number at drag crisis	
U_c	Critical velocity	
	Modelling variables	
δ	Lateral deviation of the cricket ball	
$\vec{\tau}$	Aerodynamic torque	
$\vec{L}$	Kinetic momentum	
θ	Seam-trajectory angle	
t	Time	
(x, y)	Spatial coordinates	

C_D^* (C_S^*) corresponds to drag coefficient (resp. side coefficent) plateau after drag crisis

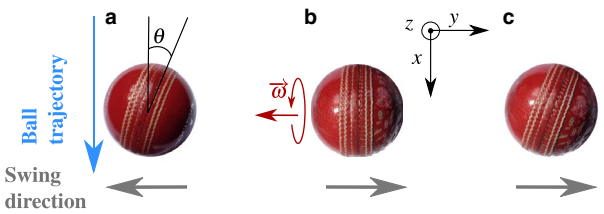

Fig. 1 Cricket ball handling for swings. **a** *Classic* swing. the ball has no roughness, but the seam is inclined with respect to throw direction. **b** *Contrast* swing. No angle between seam and throw direction, but the ball has a differential roughness. **c** *Reverse* swing. The seam is inclined to throw direction and the ball has differential roughness. The *x*-*y* frame will be used along the paper to describe the ball motion in the horizontal plane

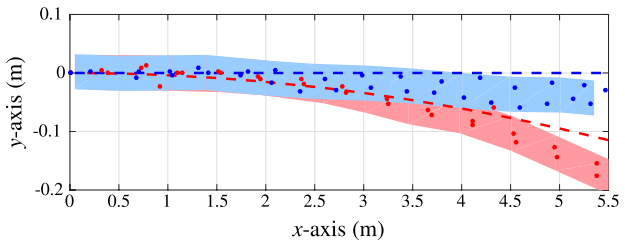

Fig. 2 Typical cricket ball trajectories (indoor conditions). (●) unworn ball, no swing. (●) Contrast swing obtained with a one-sided rough ball, $r = 1.4\,10^{-2}$. The light-coloured patches show typical measurement error on the ball's lateral position. The red dashed line is the model prediction, Eq. (8)

where $A = -1.05\,10^5$ and $B = -1.36\,10^5$ are dimensionless fitting coefficients. We use these data to predict at which launching velocity a bowler can expect to get a side force on a ball with differential roughness.

4.3 Effect of the number of launches

Using the empirical law of Eq. (11), we can predict the critical velocity at which a ball may be launched to obtain

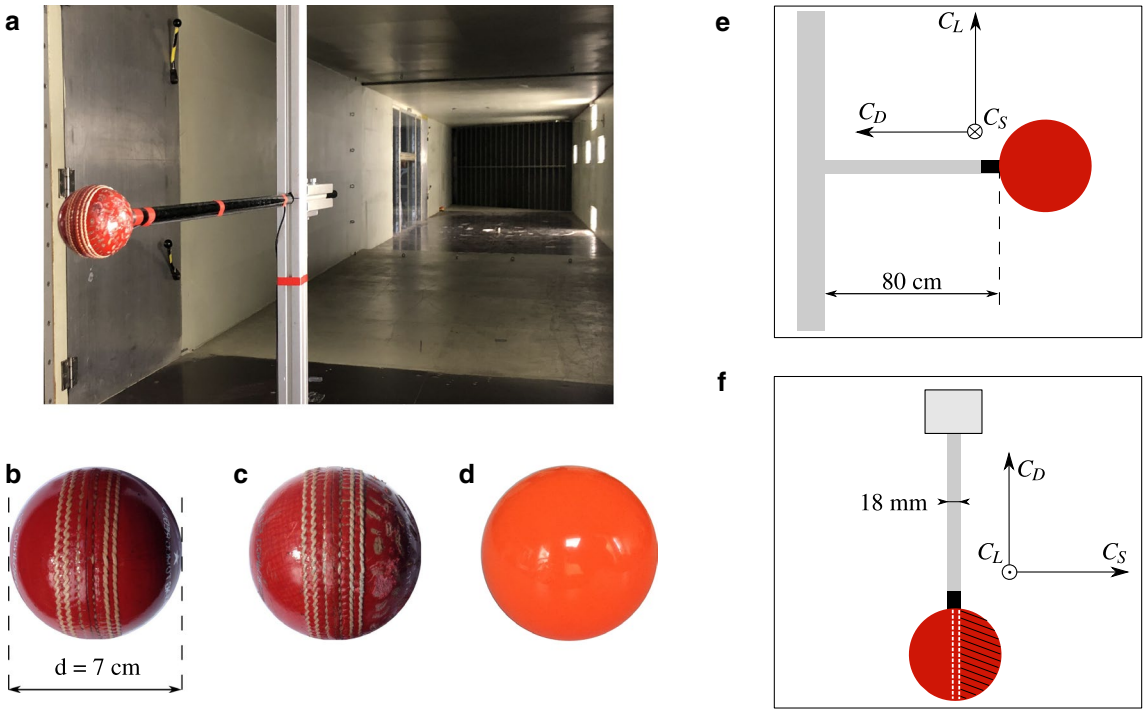

Fig. 3 Experimental material. **a** Picture of cricket ball tested in wind tunnel. **b** Smooth unworn ball. **c** One-sided rough ball. **d** Field hockey ball. **e** Lateral view of the experimental setup. The ball is separated from the pole by 80 cm. **f** Top view of the experimental setup. The sting diameter is 18 mm. The rough side of the ball corresponds to the stripped part. The black rectangle represents the force sensor

contrast or reverse swing depending on the ball roughness. The results of Fig. 7 show that, for the ball whose roughness was measured as a function of number of launches, the critical velocity decreases as wear increases. For balls with only one rough side, the higher the roughness, the lower is the critical velocity. Figure 7 demonstrates that we can obtain contrast swing at launching velocities in the range 12–40 m s^{-1} (as shown in Fig. 1) with a ball of roughness $r = 1.4\,10^{-2}$.

We use Eqs. (11), (9) and (8) to compute the lateral deviation $\delta = y(D)$ at a pitch length distance D. The results are plotted in Fig. 9. For a given lateral deviation, the larger the roughness, the lower is the launching velocity. We also indicated in Fig. 9 on which curve the reference worn ball was located after 0, 9 and 24 launches.

5 Discussion

It must be recalled that when playing cricket, the ball is not worn uniformly as in the experiments. As stated before, wear forms in patches on the ball as it hits the ground. The relationship between patchy wear and side force has not been explored yet. For instance, a rough patch near the seam may have more influence on the ball behaviour than one located at the centre of the hemisphere, as it may trigger turbulence in the boundary layer earlier than a patch located at the centre of the hemisphere. This situation is even more complex if one considers the flow acceleration between the stagnation point (near the seam) and the flow separation point (near the centre of the hemisphere). Nevertheless, the spinning of the ball might have an averaging effect on the boundary layer flow, but this has to be confirmed experimentally.

We have reported here measurements of roughness on a dry ground of similar consistency as a cricket pitch. The ground used here is slightly rougher than a real cricket pitch, but the launching velocities that we were able to reach are lower than those achievable by professional cricket bowlers. Depending on pitch conditions (cracks on the pitch for instance), the ball may wear more or less rapidly.

The influence of weather conditions on the cricket ball trajectory has been discussed in the literature. Mehta [6] showed that humidity only slightly affects swing in cricket. He also indicated the air viscosity as a possible variable for game conditions. We can use our model to further compute the influence of temperature for instance. If the game is played in cold conditions, at 5 °C for instance, the air viscosity is $\nu = 1.37\,10^{-5}$ m^2 s^{-1}. On the contrary, if the game is played in hot weather conditions, at 35 °C for instance, the air viscosity is $\nu = 1.64\,10^{-5}$ m^2 s^{-1}. The air viscosity can shift by as much as ±10% around the viscosity of air at 20 °C as

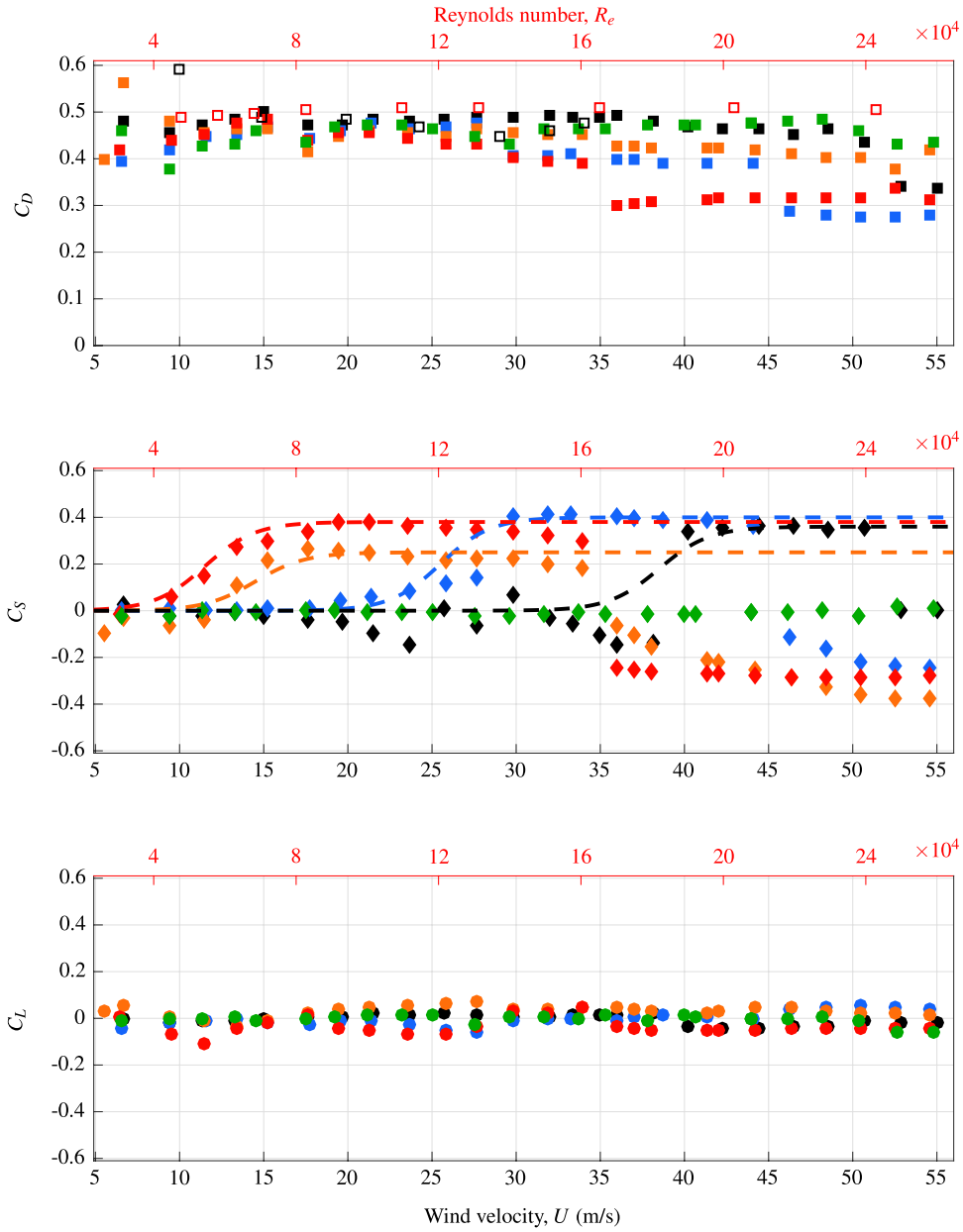

Fig. 4 Aerodynamic coefficients as a function of wind velocity (black scale) and Reynolds number R_e (red scale). (top) Drag coefficient C_D. (middle) Side force coefficient C_S. (bottom) Lift coefficient C_L. Aerodynamic forces were measured on (●) a smooth field hockey ball , (●) a new cricket ball, (●) a cricket ball with small differential roughness, (●) a cricket ball with medium differential roughness and (●) a cricket ball with large differential roughness. (□) data from Sayers et. al [16]. (□) data from Achenbach [15]. Dashed lines are fits from Eq. (9) to determine the critical wind velocity at which side force occurs

a consequence of the temperature. The increase of air viscosity with temperature tends to increase the critical launching velocity required to obtain contrast or reverse swing.

Our analysis focuses on contrast swing where the seam has little influence on the ball aerodynamics. Reverse swing is more complex, since the seam also plays a role in the aerodynamics of the ball [7, 14]. We expect that the effect of the seam and the presence of some roughness due to previous launches on the smooth side of the ball may reduce the effect presented here.

6 Conclusion

We studied the roughness effect on the curved trajectories obtained in cricket for contrast swing launches. The curved trajectory appears after the transition of the boundary layer of the rough hemisphere of the ball from laminar to turbulent. This creates a net lateral force between the two sides that moves the ball laterally. The consequent aerodynamic torque is counterbalanced by the high spinning rate of the ball fixing its orientation during the flight. The

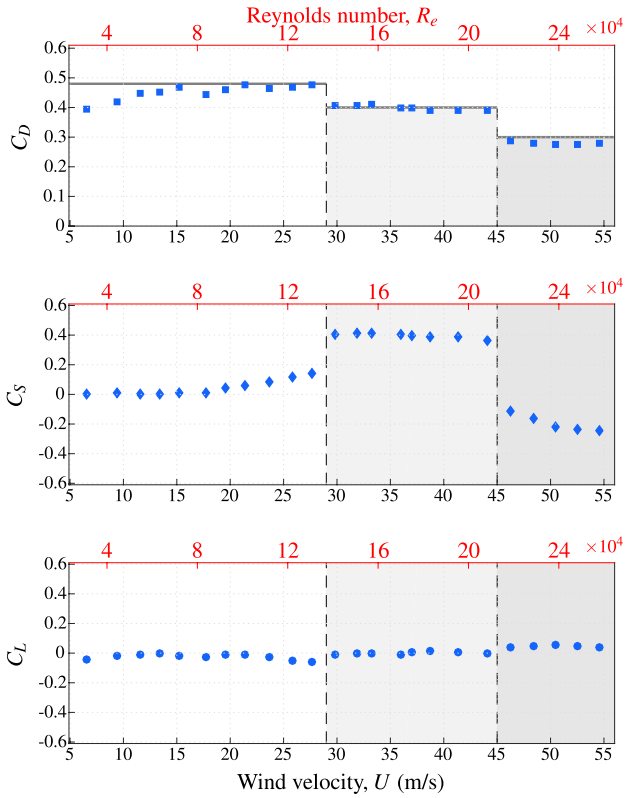

Fig. 5 Aerodynamic coefficients of a cricket ball with small differential roughness as a function of wind velocity (black scale) and Reynolds number R_e (red scale). (top) Drag coefficient C_D. (middle) Side force coefficient C_S. (bottom) Lift coefficient C_L. White region: laminar boundary layer on both sides of the cricket ball. Light grey region: turbulent boundary layer on the rough side only. Grey region: turbulent boundary layer on both sides of the cricket ball

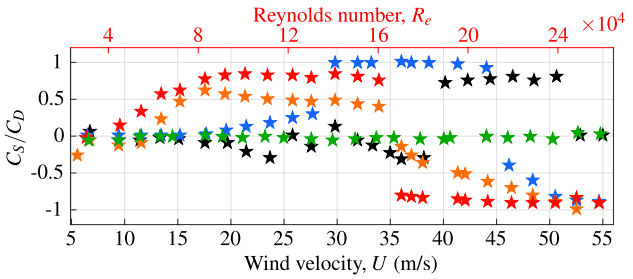

Fig. 6 C_S/C_D for different surface's roughness as a function of the wind velocity (black scale) and Reynolds number R_e (red scale). (★) Smooth field hockey ball. (★) unworn cricket ball, (★) one-sided rough cricket ball with small roughness, (★) one-sided rough cricket ball with medium roughness and (★) one-sided rough cricket ball with large roughness.

conservation of the orientation of the ball is necessary to obtain the contrast swing effect.

We showed with systematic roughness measurements, wind tunnel tests and modelling that contrast swing can be quantified. For a given bowling velocity and a given ball

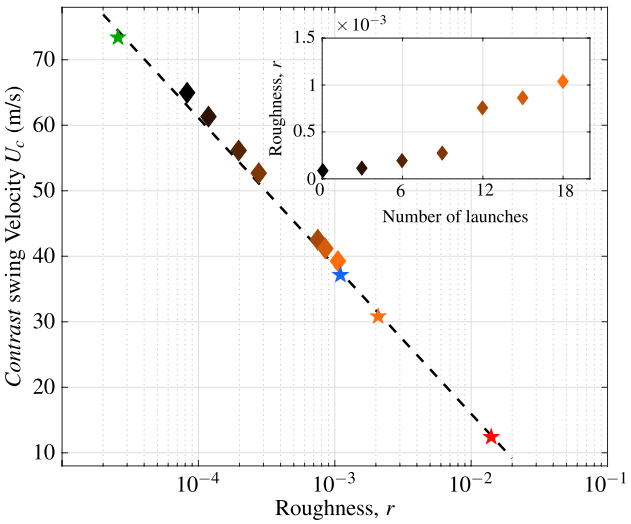

Fig. 7 Minimal launching velocity at which *contrast* swing may occur. (★) Field hockey ball made of moulded plastic. (♦) Cricket balls with different levels of wear. (★) Machined cricket balls of small roughness, (★) middle roughness and (★) high roughness. Inset : evolution of the roughness of the ball with the number of launches

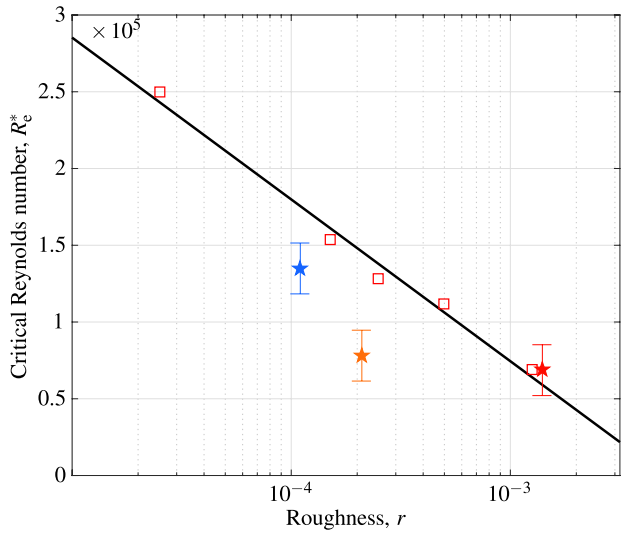

Fig. 8 Critical velocity at which drag crisis occurs on a sphere. (□) Data from Achenbach (1974). (★) Measurement of side force apparition on a small roughness, (★) middle roughness and (★) high roughness cricket balls

roughness, we can predict the lateral deviation using the two empirical laws developed in this paper. We also discussed the effect of temperature on the contrast and reverse swing of the ball: we expect those swings to appear more easily during cold conditions.

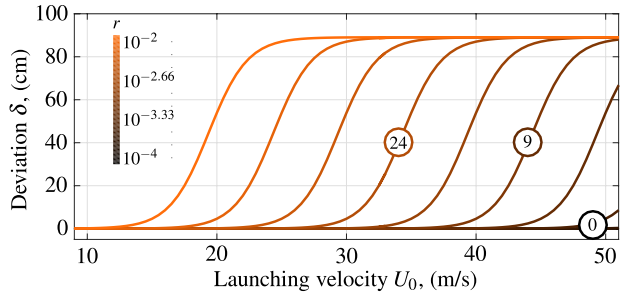

Fig. 9 Lateral deviation of a one-sided rough cricket ball as a function of the launching velocity U_0. Colour indicates the roughness r of the rough ball varying logarithmically between 10^{-4} and 10^{-2}. The corresponding number of launches to achieve a given ball roughness is indicated within circles

Acknowledgements The authors warmly thank Antonio Martinez for his help and advice regarding the measurement of roughness on cricket balls and Greg Dimitriadis for his careful proofreading of the manuscript.

Funding CHAR. RECH.-1 .B423.18. (Tadrist L.).

Compliance with ethical standards

Conflict of interest The authors declare that they have no conflict of interest.

References

1. Goff JE (2013) A review of recent research into aerodynamics of sport projectiles. Sports Eng 16(3):137–154
2. Clanet C (2015) Sports ballistics. Annu Rev Fluid Mech 47:455–478
3. Dupeux G, Le Goff A, Quéré D, Clanet C (2010) The spinning ball spiral. New J Phys 12(9):093004
4. Kray T, Franke J, Frank W (2014) Magnus effect on a rotating soccer ball at high reynolds numbers. J Wind Eng Ind Aerodyn 124:46–53
5. Mehta R, Alam F, Subic A (2008) Review of tennis ball aerodynamics. Sports Technol 1(1):7–16
6. Mehta RD (2005) An overview of cricket ball swing. Sports Eng 8(4):181–192
7. Deshpande R, Shakya R, Mittal S (2018) The role of the seam in the swing of a cricket ball. J Fluid Mech 851:50–82
8. Lock GD, Edwards S, Almond DP (2010) Flow visualization experiments demonstrating the reverse swing of a cricket ball. Proc Inst Mech Eng Part P J Sports Eng Technol 224(3):191–199
9. Alam F, La Brooy R, Subic S (2007) Aerodynamics of cricket ball-an understanding of swing. In: Fuss FK, Subic A, Ujihashi S (eds) The Impact of technology on Sport II. Taylor and Francis, United Kingdom, pp 311–316
10. Mehta R (2014) Fluid mechanics of cricket ball swing. In: 19th Australasian fluid mechanics conference
11. Mehta RD (1985) Aerodynamics of sports balls. Annu Rev Fluid Mech 17(1):151–189
12. Haake S, Goodwill S, Carre M (2007) A new measure of roughness for defining the aerodynamic performance of sports balls. Proc Inst Mech Eng Part C J Mech Eng Sci 221(7):789–806
13. Alam F, Hillier D, Xia J, Chowdhury H, Moria H, La Brooy R, Subic A (2010) Aerodynamics of used cricket balls. In: 17th Australasian fluid mechanics conference, Auckland
14. Scobie JA, Pickering SG, Almond DP, Lock GD (2013) Fluid dynamics of cricket ball swing. Proc Inst Mech Eng Part P J Sports Eng Technol 227(3):196–208
15. Achenbach E (1974) The effects of surface roughness and tunnel blockage on the flow past spheres. J Fluid Mech 65(1):113–125
16. Sayers A, Hill A (1999) Aerodynamics of a cricket ball. J Wind Eng Ind Aerodyn 79(1–2):169–182
17. Barton N (1982) On the swing of a cricket ball in flight. Proc R Soc Lond A Math Phys Sci 379(1776):109–131
18. Scobie JA, Shelley WP, Jackson RW, Hughes SP, Lock GD (2019) Practical perspective of cricket ball swing. Proc Inst Mech Eng Part P J Sports. Eng Technol. https://doi.org/10.1177/1754337119872874
19. Baker C (2010) A calculation of cricket ball trajectories. Proce Inst Mech Eng Part C J Mech Eng Sci 224(9):1947–1958
20. Korbahti B, Kagambage E, Andrianne T, Razak NA, Dimitriadis G (2011) Subcritical, nontypical and period-doubling bifurcations of a delta wing in a low speed wind tunnel. J Fluids Struct 27(3):408–426
21. Bartlett RM, Stockill NP, Elliott BC, Burnett AF (1996) The biomechanics of fast bowling in men's cricket: a review. J Sports Sci 14(5):403–424
22. Fuss FK, Lythgo N, Smith RM, Benson AC, Gordon B (2011) Identification of key performance parameters during off-spin bowling with a smart cricket ball. Sports Technol 4(3–4):159–163
23. Fuss FK, Smith RM, Subic A (2012) Determination of spin rate and axes with an instrumented cricket ball. Proc Eng 34:128–133
24. Cork A, Justham L, West A (2013) Three-dimensional vision analysis to measure the release characteristics of elite bowlers in cricket. Proc Inst Mech Eng Part P J Sports Eng Technol 227(2):116–127
25. Maccoll JW (1928) Aerodynamics of a spinning sphere. Aeronaut J 32(213):777–798
26. Barkla H, Auchterlonie L (1971) The magnus or robins effect on rotating spheres. J Fluid Mech 47(3):437–447